Spatiotemporal variations of cropland carbon sequestration and water loss across China

Shouzheng Jiang, Jie Wu, Zhihui Wang, Ziling He, Mingjun Wang, Weiwei Yao, Yu Feng

Agricultural Water Management 287 (2023) 108427

Contents lists available at ScienceDirect

Agricultural Water Management

journal homepage: www.elsevier.com/locate/agwat

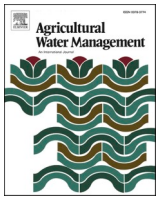

Spatiotemporal variations of cropland carbon sequestration and water loss across China

Shouzheng Jiang [a], Jie Wu [b,c,*], Zhihui Wang [a], Ziling He [a], Mingjun Wang [a], Weiwei Yao [a], Yu Feng [b,d,**]

[a] State Key Laboratory of Hydraulics and Mountain River Engineering & College of Water Resource and Hydropower, Sichuan University, Chengdu, China
[b] School of Environmental Science and Engineering, Southern University of Science and Technology, Shenzhen, China
[c] Department of Geoscience and Natural Resource Management, University of Copenhagen, Copenhagen, Denmark
[d] Laboratoire des Sciences du Climat et de l'Environnement, UMR 1572 CEA-CNRS-UVSQ, Gif-sur-Yvette, France

ARTICLE INFO

Handling Editor - Z. Xiying

Keywords:
Water use efficiency
Water and carbon exchange
Non-paddy field
Paddy field
MODIS data

ABSTRACT

Croplands play a critical role in regulating terrestrial water and carbon cycles and provide essential social services for humans. Investigating the characteristics of water and carbon flux in cropland ecosystems offers valuable information for advancing sustainable agriculture management. Combining the up-to-date Moderate Resolution Imaging Spectroradiometer and cropland distribution data, this study quantified the temporal-spatial variations of evapotranspiration (ET), gross primary productivity (GPP), and ecosystem-scale water use efficiency (WUE) in paddy (PF) and non-paddy field (NPF) over China from 2000 to 2021. The results showed that annual ET in both PF and NPF presented an increasing trend from northwest to southeast of China, with mean annual ET totaling 625 ± 43 mm yr^{-1} and 487 ± 45 mm yr^{-1} in PF and NPF, respectively. The Sen's slope showed that annual ET presented significantly increasing trends ($p < 0.01$), with a rate of $66.7^{+10.9}_{-12.2}$ mm yr^{-1} $decade^{-1}$ in NPF and $59.8^{+16.6}_{-14.9}$ mm yr^{-1} $decade^{-1}$ in PF. The magnitudes of the increase in annual ET mainly came from the ET increase in summer, with the quantified contribution rates of 38.4 % in PF and 50.74 % in NPF. The spatial variations of cropland annual GPP agreed well with that of annual ET. The mean annual GPP in PF and NPF was estimated at 1029 ± 57 gC m^{-2} yr^{-1} and 776 ± 67 gC m^{-2} yr^{-1} from 2000 to 2021, respectively, along with its significantly increasing trend at $84.0^{+15.9}_{-14.2}$ gC m^{-2} $decade^{-1}$ and $96.3^{+14.2}_{-9.7}$ gC m^{-2} $decade^{-1}$ ($p < 0.01$) in PF and NPF during this period, respectively. The increase in spring GPP mainly contributed to the increasing annual GPP in PF. In contrast, the rising GPP in spring and summer primarily resulted in the increasing annual GPP in NPF. The mean annual WUE is 1.65 ± 0.05 gC m^{-2} $kg^{-1}H_2O$ in PF and 1.59 ± 0.03 gC m^{-2} $kg^{-1}H_2O$ in NPF, respectively. The investigations of the variations of WUE demonstrated that both PF and NPF experienced negative trends in China, but the trends were not uniform, and disparities existed across the sub-agricultural districts. The quantified spatial and temporal patterns of how croplands trade water for carbon will help better manage agricultural water resources and ensure food security.

1. Introduction

Croplands can provide not only food for humans and livestock, but also critical social services, such as fiber, wood products, etc. (Lan et al., 2021b). However, the cropland area is limited and tends to decrease in some regions due to rapid degradation, urbahnization and industrialization (Ju et al., 2013). Thus, increasing productivity on existing arable lands was considered to be a more feasible option for enhancing future food security (Ai et al., 2020). One of the problems in agricultural intensification is the need to consider the trade-off between cropland carbon sequestration and water consumption. China accounts for about 7 % of the world's existing arable lands, but feeds 22 % of the world's population (Piao et al., 2010). Meanwhile, the fast-growing population is driving a fast-growing demand for food supply (Feng et al., 2021). Accurately quantifying cropland productivity and its water use status in climate change is essential to guaranteeing China's food security and

* Corresponding author at: School of Environmental Science and Engineering, Southern University of Science and Technology, Shenzhen, China.
** Corresponding author.
E-mail addresses: jw@ign.ku.dk (J. Wu), yu.feng@lsce.ipsl.fr (Y. Feng).

https://doi.org/10.1016/j.agwat.2023.108427
Received 21 April 2023; Received in revised form 1 June 2023; Accepted 19 June 2023
Available online 23 June 2023

sustainable agriculture development (Piao et al., 2010).

Global warming exhibited a notable increasing trend from 2001 to 2020, which will continue to rise as reported by IPCC (https://www.ipcc.ch/report/sixth-assessment-report-cycle/). Meanwhile, the temperature in China increased at a rate of 0.24 °C per decade during the last two decades (Ferreira and Cunha, 2020). At the same time, multiple lines of evidence indicate widespread greening in China due to the combined effects of CO_2 fertilization and rising temperature (Keenan et al., 2013; Piao et al., 2020). Global estimates showed that China, with 6.6 % of global vegetated lands, comprised one-quarter of the global greening during 2000–2017 (Chen et al., 2019). Among them, cropland accounts for 32 % of the greening due to intensive management over the past 30 years (Forzieri et al., 2020). The changes in climate and vegetation have been proven to alter the regional carbon, energy, and water fluxes (Zeng et al., 2018a; Wu et al., 2022a; Jin et al., 2022). Many observational studies have investigated cropland ecosystem water and carbon exchange process by field measurements (i.e., eddy covariance) (Jiang et al., 2020a; Liang et al., 2022; Wu et al., 2022b; Feng et al., 2017a, 2017b), which made substantial progress in understanding the water and carbon cycle between land and atmosphere at the site scale, but the long-term spatial-temporal patterns of water and carbon patterns still lacking (Jin et al., 2017). With the development of satellite observations, Moderate Resolution Imaging Spectroradiometer (MODIS) satellite products have been widely used in the large-scale assessment of gross primary productivity (GPP) and evapotranspiration (ET) process (Cheng et al., 2021; He et al., 2020), which provides an opportunity to estimate the carbon sequestration and water flux over large spatio-temporal scales in the context of climate and underlying vegetation changes (Yuan et al., 2020).

Terrestrial ET and GPP generally presented increasing trends in recent decades globally, while their regional trajectories remain controversial due to the complex interactions between soil, vegetation, and climate (Ogutu et al., 2021; Yang et al., 2021). ET in China significantly increased at 10.7 mm yr^{-1} $decade^{-1}$ over the past 30 years ($p < 0.05$), and the largest magnitude ($>$ 60 mm yr^{-1} $decade^{-1}$) occurred in the eastern Sichuan, southern Taiwan, and central China, attributed to temperature and solar radiation increase, as well as the increased vegetation activity (Li et al., 2018). Cheng et al. (2021) also reported a comparable increasing ET trend in China, with an average rate of 29.5 mm yr^{-1} $decade^{-1}$ in 2001–2018, and exhibited differences in various seasons and for different vegetation types. Bai et al. (2019) detected a significant increasing ET in a typically hilly-gully basin on the Loess Plateau, and found $>$ 90 % of the ET trend can be explained by vegetation greening. In addition, the GPP increment is widely spread with 60 % area showing significant increasing trend ($p < 0.05$) in China during 1982–2015, with the largest increase in GPP (>60 gC m^{-2} yr^{-1} $decade^{-1}$) occurred in densely forested area in Yunnan in the Southeast, southeast of Tibetan Plateau, Daxing'anling in the Northeast and Taiwan Island (Yao et al., 2018). National or regional terrestrial water and carbon flux research was mainly focused on the grassland and forest of China (Bai et al., 2019), where widespread greening alters the bio-geophysical processes due to afforestation and ecology conservation affecting vegetation cover (i.e., Grain for Green in the Loess Plateau, the Three-north Forest Shelterbelt Project in the north of China). As a consequence of climate change, as well as agricultural intensification, including multiple cropping (Chen et al., 2019), fertilizer utilization (Jin et al., 2018) and various irrigation practices (Lan et al., 2021b), rising vegetation cover was also found in China cropland. Yet, the quantified response of ET and GPP to such environmental and vegetation change has not been explored in China's croplands (Lan et al., 2021b). Besides, compared to non-paddy field (NPF), paddy field (PF) consume additional water and generally possess higher GPP, and therefore have different biophysical and biochemical feedbacks. The different responses of the carbon and water flux to such change remain unclear.

Water use efficiency (WUE), defined as the ratio of GPP to ET, has been recognized as a vital indicator to investigate the coupled relationship between water consumption and crop production, and to reflect how ecosystems adapted to environmental and climate change (Hussain et al., 2019). Therefore, analyzing the spatiotemporal variations of cropland WUE is beneficial for agricultural water management and sustainable agricultural development. As GPP and ET are strongly linked, whether such a coupling effect can lead to an offset between ET and GPP on WUE remain unclear. Besides, the variability of WUE is subject to considerable uncertainties due to the different water management (PF versus NPF) and environmental variables in China. However, the trend of WUE remains poorly understood for China's cropland at a large scale, particularly the comparison between PF and NPF WUE has not been previously explored.

Totally, there still a lack of consensus on water and carbon dynamics and the coupled results between the two under climate and underlying vegetation changes in China's cropland. Quantifying such carbon–water changes is important to sustainable agricultural development and a safe future for water availability and food production (Cheng et al., 2017). In this study, we used the GPP and ET derived from the MODIS data to investigate: 1) the interannual and seasonal dynamics of GPP, ET, WUE and their spatial distribution patterns in China croplands, 2) the difference between PF and NPF and their implications for agricultural water management in China.

2. Material and methods

2.1. Study area and cropland distribution

China has 177 million hectares of cropland area, and the area is distributed throughout nine agricultural districts, including Northeast China Plain (NCP), Yunnan-Guizhou Plateau (YGP), Northern arid and semiarid region (NASR), Southern China (SC), Sichuan Basin and surrounding regions (SB), Middle-lower Yangtze Plain (MYP), Qinghai Tibet Plateau (QTP), Loess Plateau (LP) and Huang-Huai-Hai Plain (HHP). The spatial distribution of the agricultural districts can be found in Fig. S1.

Cropland distribution data are downloaded from the Resource and Environment Science and Data Center (https://www.resdc.cn/data.aspx?DATAID=99). The dataset provides the spatial distribution of croplands at 1 km resolution for 2010. Cropland is further subdivided into PF and NPF. PF refers to cultivated land with guaranteed water sources and irrigation facilities, which can be irrigated normally in ordinary years for the cultivation of aquatic crops such as rice and lotus root, cultivated land in rotation between rice and rainfed crops was also included; NPF can be divided into four types of cultivated land, including (1) cultivated land without irrigation water source and facilities, and crop growth completely depends on precipitation; (2) dry crop cultivated land with water sources and irrigation facilities, which can be irrigated normally under normal circumstances; (3) cultivated land mainly for vegetable cultivation; (4) fallow land and rest land for normal crop rotation. There are 131 Mha of NPF and 46 Mha of PF in China. The spatial distribution of the PF and NPF can be found in Fig. 1a. NPF is mainly concentrated in North China (including NCP, NASR, and HHP), accounting for 61.7 % of the national NPF area (Fig. 1b). PF is mainly concentrated in the South of China (including MYP, YGP, and SB), accounting for 73.13 % of national PF area. QTP has a negligible cropland area, and thus this region was excluded from the data analysis.

2.2. MODIS data and calculation

We use MODIS GPP and ET data from 2000 to 2021 for the analysis in this study. The data consist of the GPP product of MOD17A2H developed by the light-use efficiency model (Running et al., 2004) and the ET product of MOD16A3 based on the improved P-M algorithm (Mu et al., 2011). Both MODIS products were at 500 m spatial resolution with an 8-d temporal interval. The estimation of GPP in MODIS products is described as follows:

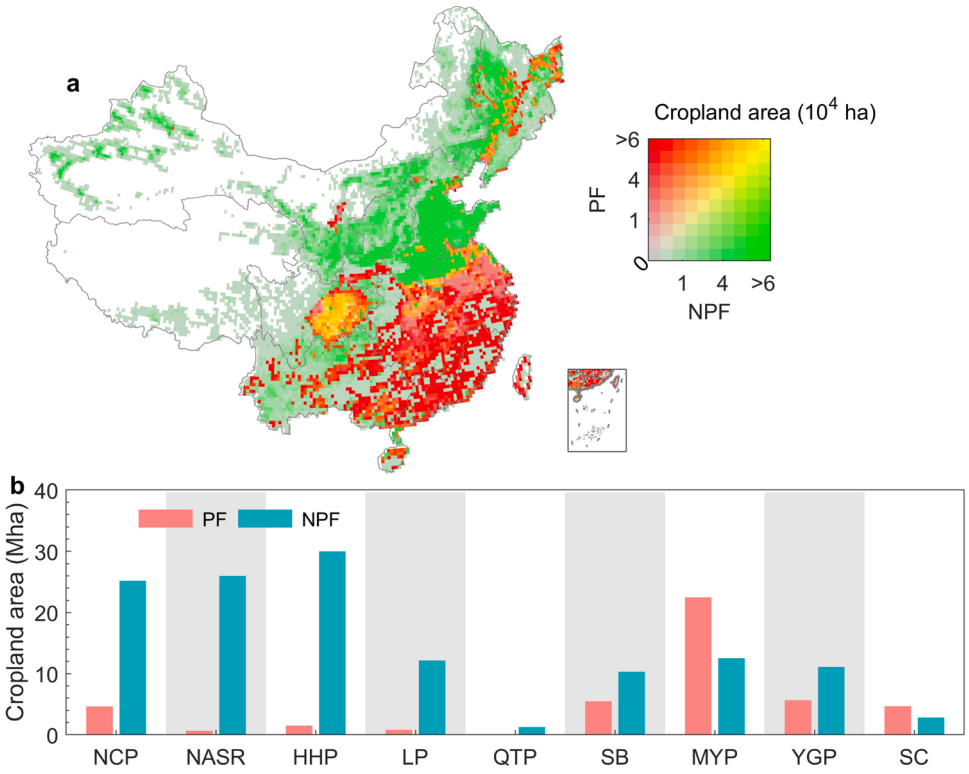

Fig. 1. Patterns of paddy filed (PF) and non-paddy field (NPF) in nine agricultural districts of China. (a) Spatial distribution. (b) Total land area.

$$GPP = \varepsilon_{\max} \times APAR \times VPD_s \times T_s \tag{1}$$

where ε_{max} is the maximum light use efficiency of the crop to convert the intercepted photosynthetically active radiation into assimilate without environmental constraints (gC m^{-2} MJ^{-1}), VPD_s and T_s represent the vapor pressure deficit and temperature constraint on crop photosynthetic activity (unitless), respectively.

$$T_s = \begin{cases} 0 & T_{min} < 0 \\ \dfrac{(T_a - T_{min})}{(T_{max_{min}} - T_{min})} & T_{min} \le T_a \le T_{max} \\ 1 & T_a > T_{opt} \end{cases} \tag{2}$$

$$VPD_s = \begin{cases} 0 & VPD > VPD_{max} \\ \dfrac{(VPD_{max} - VPD)}{(VPD_{max} - VPD_{min})} & VPD_{min} \le VPD \le VPD_{max} \\ 1 & VPD < VPD_{min} \end{cases} \tag{3}$$

where VPD is the average vapor pressure deficit (kPa), VPD_{min} and VPD_{max} are constants representing the lower and upper limits of VPD on plant photosynthesis. T_{maxmin} is the daily minimum temperature at which LUE = ε_{max}.

The estimation of ET in MODIS products is calculated as follows:

$$\lambda ET = \lambda E_i + \lambda T_c + \lambda E_s \tag{4}$$

where λE_i, λT_c and λE_s represent the latent heat of canopy evaporation of intercepted precipitation, crop transpiration and bara soil evaporation, respectively. The three components are calculated as follows:

$$\lambda E_i = \frac{\left(\Delta \times A_c \times f_c + \rho_a \times C_p \times VPD \times \frac{f_c}{r_{aw}}\right) \times F_w}{\Delta + \frac{P_a \times C_p \times r_{sw}}{\lambda \times \Delta \times r_{aw}}} \tag{5}$$

$$\lambda T_c = \frac{\left(\Delta \times A_c \times f_c + \rho_a \times C_p \times VPD \times \frac{f_c}{r_a}\right) \times \left(1 - F_w\right)}{\Delta + \gamma \times \left(1 + \frac{r_s}{r_a}\right)} \tag{6}$$

$$\lambda E_s = \lambda E_{wet} + \lambda E_{pot} \times \left(\frac{RH}{100}\right)^{\frac{VPD}{\beta}} \tag{7}$$

where Δ denotes the saturation water vapor pressure-temperature curve slope (kPa· ℃$^{-1}$), A_c represents the canopy available energy (W m^{-2}), f_c represents the canopy cover fraction (unitless), ρ_a represents the air density (kg m^{-3}), C_p represents the air specific heat capacity, VPD represents the water vapor pressure deficit (kPa), F_w represents the wet canopy surface fraction (unitless), P_a represents the air pressure, r_{aw} and r_{sw} is the aerodynamic resistance and wet canopy resistance to the evaporated water on the wet canopy surface (s m^{-1}), respectively, r_a and r_s is the aerodynamic resistance and dry canopy resistance (s m^{-1}), respectively. λE_{wet}denotes the evaporation from wet soil (W m^{-2}), λE_{pot}denotes the potential soil evaporation (W m^{-2}), RH denotes the relative humidity (%), β is a constant and set to 200. Detailed descriptions of MODIS GPP and ET calculations can be found in previous studies (Monteith, 1965; Mu et al., 2007; Mu et al., 2011).

Cropland WUE is calculated as the ratio of GPP to ET per pixel (WUE=GPP/ET) from 2000 to 2021.

2.3. Data analysis and statistics

2.3.1. Theil-Sen estimator

We quantified the trends in GPP, ET, and WUE employing the non-parametric Theil–Sen method (TSA; Sen, 1968). The TSA is one of the widely used methods to quantify the magnitude of the trend in time series (Feng et al., 2022). TSA slope is calculated as the trend slope of sequence β:

$$\beta = Median\left(\frac{x_i - x_j}{i - j}\right), \forall 1 < i < j \tag{8}$$

where β denotes the Theil-Sen estimator, x_i and x_j represent the value corresponding to time i and j, respectively. In the present study, annual and seasonal changes of the ET, GPP and WUE in their magnitude and trend were estimated for the whole region and the various agricultural districts from 2000 to 2021.

2.3.2. Mann-Kendall trend test

The significance of the trends in time-series (i.e., GPP, ET, and WUE) was tested employing the non-parametric Mann-Kendall (M-K) method. The M-K method has the advantage that it does not require the samples to follow a normal distribution. In addition, the method is not seriously influenced by the actual distribution of the data and is less sensitive to outliers. For the trend test, the M-K was depended on the statistic S (Mann, 1945), and it is estimated as:

$$S = \sum_{k=1}^{n=1} \sum_{j=k+1}^{n} \mathrm{sgn}(x_i - x_j) \tag{9}$$

where n is the sample size, x_i and x_j represent the data value corresponding to time i and j (j > i), respectively. sgn (x_i-x_j) is calculated as:

$$\mathrm{sgn}(x_i - x_j) = \begin{cases} 1 & \text{if}(x_i - x_j) \langle 0 \\ 0 & \text{if}(x_i - x_j) = 0 \\ -1 & \text{if}(x_i - x_j) \rangle 0 \end{cases} \tag{10}$$

That is, each value is compared to an adjacent to determine whether the latter is larger than the former. If the sample size n ≥ 10, the statistic S approximately follows the standard normal distribution, the mean value is theoretically 0, namely E(S)= 0, and its variance (Var (S)) is estimated as follows:

$$Var(S) = \frac{\left[n(n-1)(2n-5) - \sum_{m=1}^{n} t_m(t_m-1)(t_m+5)\right]}{18} \tag{11}$$

Where t_m is the number of ties of extent m, and $\sum_{m=1}^{n}$0denotes the summation over all ties. A normalized test statistic Z is computed using the following equation:

$$Z = \begin{cases} \dfrac{S-1}{\sqrt{\mathrm{Var}(S)}} & \text{if} S > 0 \\ 0 & \text{if} S = 0 \\ \dfrac{S+1}{\sqrt{\mathrm{Var}(S)}} & \text{if} S < 0 \end{cases} \tag{12}$$

where Z is the test statistics, which is adopted to detect whether the increasing (positive value) or decreasing (negative value) monotonic trends are significant at a specific α level. The hypothesis that there is no significant trend was rejected if $|Z| > Z_{1-\alpha/2}$. The significance level α = 0.05 (or 95 % confidence intervals) and α = 0.01 (or 99 % confidence intervals) were used to test the significant trend of the variables (i.e., GPP, ET, and WUE) at an annual and seasonal time-step from 2000 to 2021 in each pixel.

3. Results

3.1. Spatiotemporal variation of ET

The spatial-temporal patterns of mean annual ET in the PF and NPF of China from 2000 to 2021 are displayed in Fig. 2 and Fig. 3. In general, ET in the southern part of China is higher than in the northern part for both PF and NPF (Fig. 2). The mean annual ET in PF is averaged at 625 ± 43 mm yr^{-1}, which is larger than the value of 487 ± 45 mm yr^{-1} in NPF (Fig. 3b) over the study period. The difference between PF and NPF ET is more evident in the agricultural districts located in North China, especially in LP, where the difference is larger than 150 mm yr^{-1} (Fig. 3d). Seasonally, ET in summer accounts the most of the annual ET amount in both PF and NPF, followed by spring, autumn and winter (Fig. S2). Regionally, there are large spatial heterogeneities of annual and seasonal ET across several agricultural districts (Fig. 2 and Fig. S2). The mean annual ET values of different agricultural districts vary between 352 and 757 mm yr^{-1} for PF, and 346–827 mm yr^{-1} for NPF. Overall, annual ET in both PF and NPF increases from northwest to southeast of China, with the highest annual ET in SC and lowest value in NASR (Fig. 2, Fig S2).

In terms of temporal dynamics, annual ET in both PF and NPF experienced significantly increasing trends in China and its eight agricultural districts ($p < 0.01$; M-K test) over the study period (Fig. 3a, c). The TSA shows the increasing rate of NPF ET is $66.7^{+10.9}_{-12.2}$ mm yr^{-1} $decade^{-1}$ (subscript and superscript values present the 95 % confidence interval; M–K test; $p < 0.05$), while the value is $59.8^{+16.6}_{-14.9}$ mm yr^{-1} $decade^{-1}$ in PF (Fig. 3b). Annual ET in NPF has higher rising rate than in PF in China and all agricultural districts except for LP (Fig. 3c), confirming the faster increase in NPF ET throughout China. Regionally, large spatial heterogeneities in seasonal and annual ET trends are observed (Fig. 4). For example, the magnitudes of upward annual ET in the LP and SB are evidently higher than in other districts, with a positive rate of approx. 100 mm yr^{-1} $decade^{-1}$ (Fig. 3c). Although the rate of ET trends in southern parts of China is lower than in the north (e.g., LP), the south has the biggest PF area, making the south contribute to most of China's PF ET increase (85.0 %). For NPF, the north contributes to most of China's ET increase (66.8 %). Seasonally, summer ET primarily drives the increase in annual ET, with the contribution rate of 38.4 % in PF and 50.8 % in NPF, followed by spring (32.1 % and 29.1 %) and autumn (23.7 % and 18.8 %), while the contribution in winter is ignorable (5.8 % and 1.4 %) (Fig. S3, Table 1).

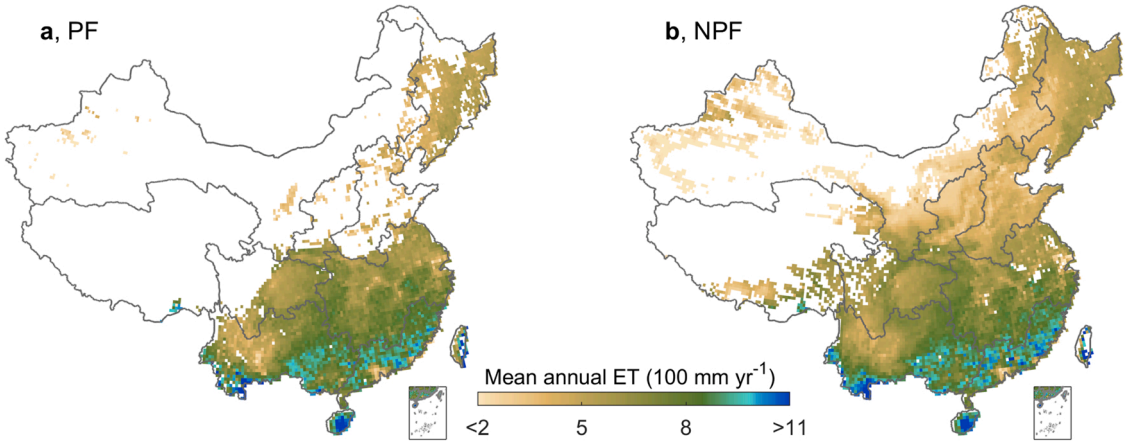

Fig. 2. Spatial variability of mean annual evapotranspiration (ET) in (a) paddy field and (b) non-paddy field of China over the period of 2000–2021.

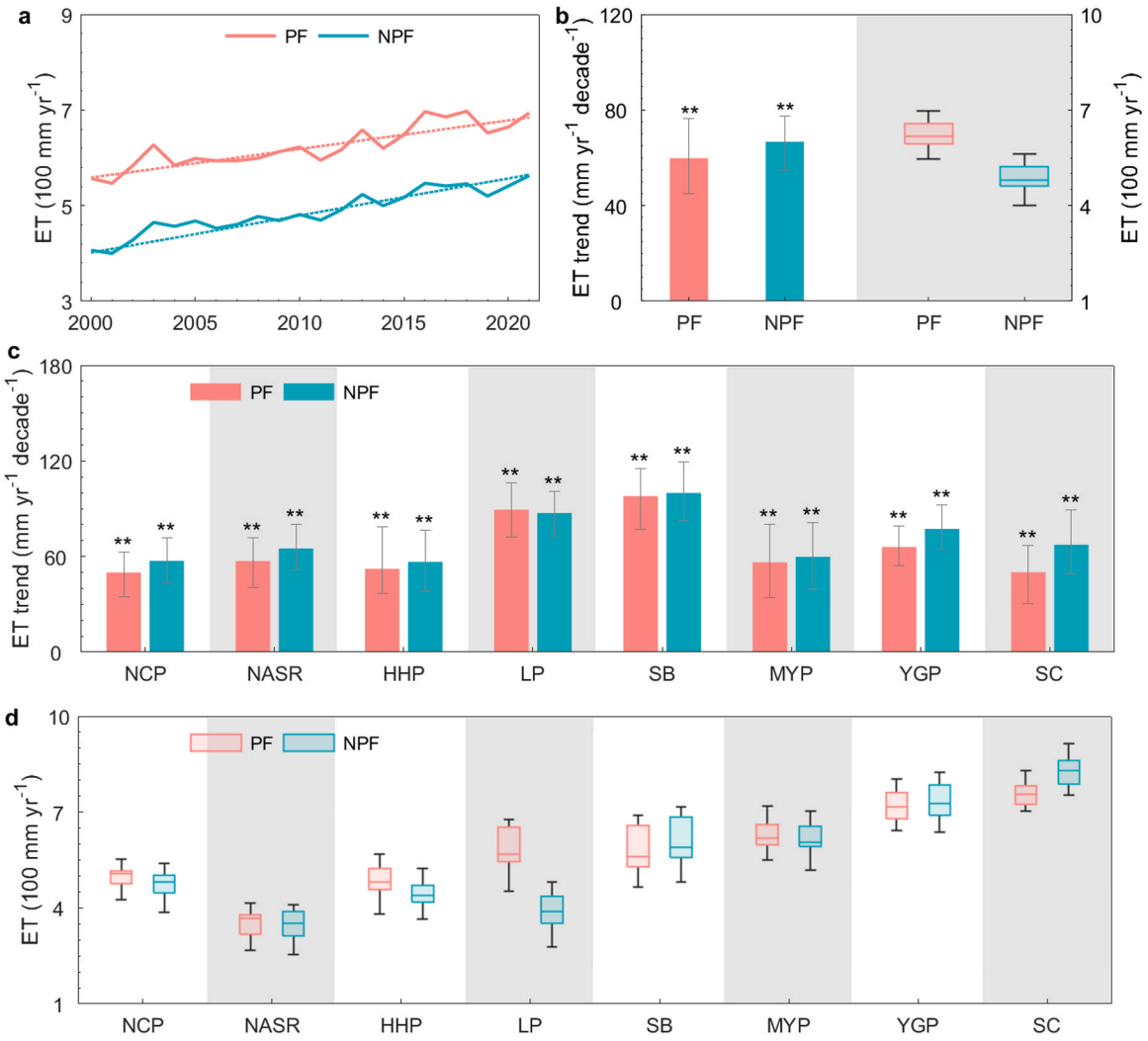

Fig. 3. Amount and trends in annual evapotranspiration (ET) in paddy field (PF) and non-paddy field (NPF) over China during 2000–2021. (a) Time-series of annual ET over whole China. (b) Trends and amount of ET over whole China. c-d, Trends (c) and amount (d) of ET in nine agricultural districts. The error bars in b and c represent standard error of the trends, and * * represents significant ET changes ($p < 0.01$) based on the Mann-Kendall trend test.

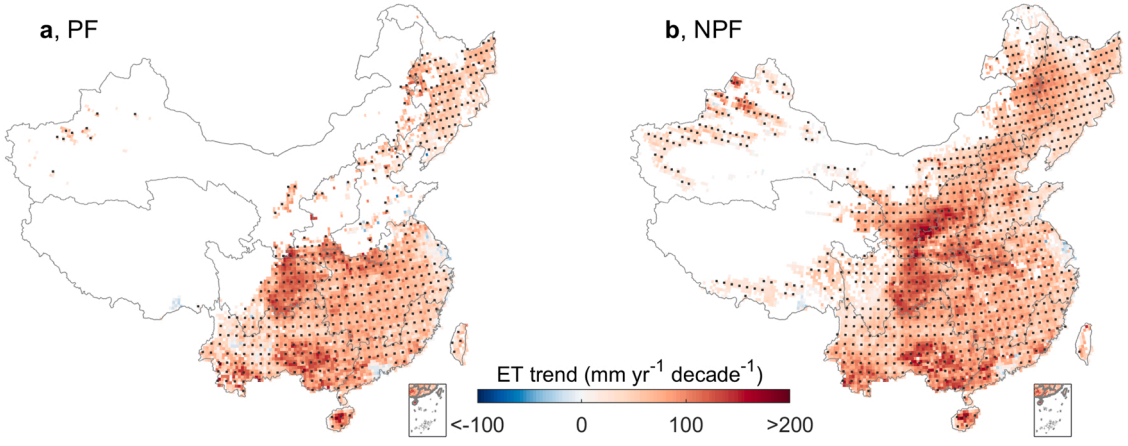

Fig. 4. Spatial patterns of trends in annual evapotranspiration (ET) in (a) paddy field (PF) and (b) non-paddy field (NPF) of China over the period of 2000–2021. The dotted grids represent significant ET changes ($p < 0.05$) based on the Mann-Kendall trend test.

3.2. Spatiotemporal variation of GPP

The spatial distribution and trend of annual GPP in the PF and NPF are shown in Figs. 5–7. The mean annual GPP is 1029 ± 57 gC m^{-2} yr^{-1} in PF, but the value (776 ± 67 gC m^{-2} yr^{-1}) is lower in NPF of China (Fig. 6b). The spatial variations of annual GPP are similar to that of ET

Table 1
Contributions (in %) of seasonal paddy field (PF) and non-paddy field (NPF) evapotranspiration (ET) variation across the nine agricultural districts to total ET change of China cropland.

Types	Season	Nine agricultural districts of China									China
		NCP	NASR	HHP	LP	QTP	SB	MYP	YGP	SC	
PF	Spring	1.3	0.2	0.8	0.9	0.0	6.7	16.0	4.5	1.7	32.1
	Summer	6.2	0.9	1.4	1.3	0.0	7.5	16.5	2.9	1.6	38.4
	Autumn	0.8	0.2	0.5	0.4	0.0	4.3	11.1	4.2	2.1	23.7
	Winter	0.0	0.0	0.0	0.0	0.0	0.4	1.2	2.1	2.1	5.8
NPF	Spring	2.4	4.0	7.5	2.9	0.2	4.1	4.0	3.5	0.5	29.1
	Summer	11.6	12.1	9.1	7.0	0.3	5.0	2.6	2.5	0.5	50.8
	Autumn	2.7	3.4	3.1	1.8	0.1	2.6	1.8	2.7	0.6	18.8
	Winter	-0.1	0.1	-0.8	0.0	0.1	0.3	0.2	1.3	0.5	1.4

Note: Northeast China Plain (NCP), Yunnan-Guizhou Plateau (YGP), Northern arid and semiarid region (NASR), Southern China (SC), Sichuan Basin and surrounding regions (SB), Middle-lower Yangtze Plain (MYP), Qinghai Tibet Plateau (QTP), Loess Plateau (LP) and Huang-Huai-Hai Plain (HHP).

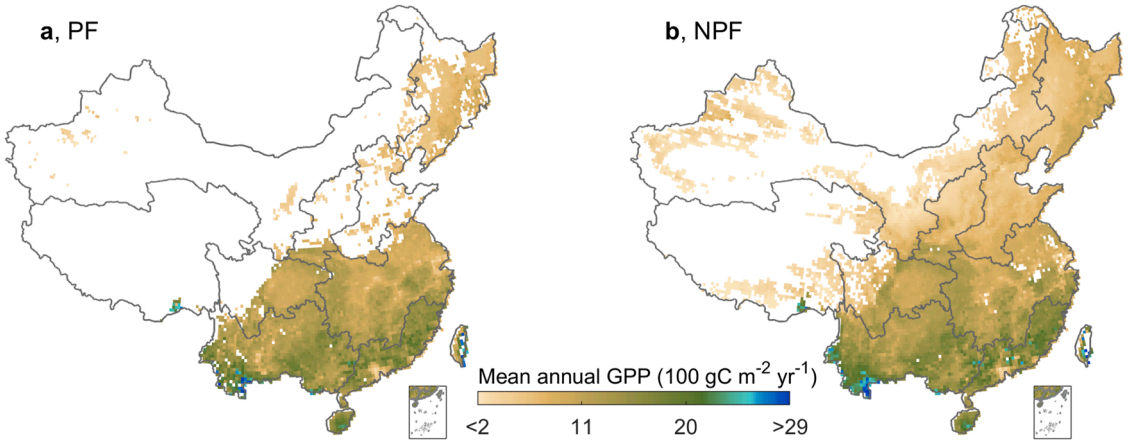

Fig. 5. Spatial variability of mean annual gross primarily productivity (GPP) in (a) paddy field (PF) and (b) non-paddy field (NPF) of China over the period of 2000–2021.

(Figs. 2 and 5), i.e., GPP increases from northwest to southeast of China, with the higher annual values (approx. 1500 gC m^{-2}) in SC, and the relatively the lower value (approx. 400 gC m^{-2}) in NASR (Fig. 6d). Annual GPP in PF is evidently higher than that of NPF in LP, where the annual GPP in PF is 2 times higher (Fig. 6d). Seasonally, similar to that of ET, summer GPP contributed the most for annual GPP in both PF and NPF, followed by spring, autumn and winter (Fig. S4).

The TSA shows that the annual GPP in China increases at a significant rate of $84.0^{+15.9}_{-14.2}$ gC m^{-2} $decade^{-1}$ in PF, and $96.3^{+14.2}_{-9.7}$ gC m^{-2} $decade^{-1}$ ($p < 0.01$) in NPF from 2001 to 2021 (Fig. 6a). The spatial patterns of the increasing trends in annual GPP were similar to that of annual ET (Fig. 7). Meanwhile, the increased GPP of PF in Southern China contributed the most for annual PF GPP (86.2 %), while the increases of the NPF in Northern China contributed the most to GPP increase in NPF (65.4 %). The sustained increase in GPP shows that both PF and NPF in China had become more productive. Similar positive trends are observed in the various agricultural districts, however, the increases in annual GPP exhibited substantial spatial variations due to different meteorological and land surface conditions across the various districts (Figs. 6 and 7), with the larger magnitudes of increase in LP and SB, and the lower in the NCP. Besides, the dynamics of GPP are also different in different seasons for both PF and NPF (Fig. S5). The magnitudes of increase in spring GPP are mainly responsible for increased annual GPP in PF (36.8 %), followed by autumn (25.8 %), summer (20.2 %) and winter (17.2 %) (Fig. S5a), while the larger increases of GPP in summer contributed the most for increased annual GPP in NPF (41.1 %), followed by spring (29.2 %), autumn (21.1 %) and winter (8.6 %) (Fig. S5b, d, Table 2).

3.3. Spatiotemporal variation of WUE

As shown in Fig. 8, the spatial patterns of the mean annual WUE show large spatial variations. Annual cropland WUE in southern China is generally higher than that of northern China. The mean annual WUE is 1.65 ± 0.05 and 1.59 ± 0.03 gC $kg^{-1}H_2O$ in PF and NPF, respectively (Fig. 9b). Totally, the WUE in NPF is comparable to that of PF in China and its agricultural districts except for LP, where WUE in PF (1.82 ± 0.05 gC $kg^{-1}H_2O$) is evidently higher than NPF (1.56 ± 0.05 gC $kg^{-1}H_2O$) (Fig. 9d). Regionally, the highest annual WUE appears in the west of YGP, where pixel-level WUE can be larger than 4 gC $kg^{-1}H_2O$, with regional mean WUE being 1.86 ± 0.05 gC $kg^{-1}H_2O$ in PF and 1.96 ± 0.05 gC $kg^{-1}H_2O$ in NPF. Seasonally, summer WUE is the highest in both PF and NPF, followed by spring, autumn and winter (Fig. S6).

Over the study period of 2000–2021, annual WUE in both PF and NPF presents a decreasing trend, but the trends are not statistically significant (Fig. 9a, b). Notably, both GPP and ET increase significantly (Figs. 3c and 6c), the larger enhancement in ET than GPP during the study period explains the decrease in WUE. The historical trends of annual WUE in PF and NPF are -0.0285 gC $kg^{-1}H_2O$ $decade^{-1}$ and -0.0072 gC $kg^{-1}H_2O$ $decade^{-1}$, respectively (Fig. 9b). Spatially, the trend of annual WUE in cropland shows larger spatial variability across the eight districts (Fig. 10). Significant decreasing trend of annual WUE is found in the cropland located in YGP, at a rate of $-0.032^{+0.032}_{-0.031}$ gC $kg^{-1}H_2O$ $decade^{-1}$ in PF and $-0.033^{+0.020}_{-0.033}$ gC $kg^{-1}H_2O$ $decade^{-1}$ in NPF, respectively ($p < 0.05$, Fig. 9c). Besides, the annual WUE of PF in NASR and LP also show significant decreasing trends ($p < 0.05$ or 0.01), with the rate of $-0.027^{+0.025}_{-0.035}$ gC $kg^{-1}H_2O$ $decade^{-1}$ and $-0.058^{+0.036}_{-0.029}$ gC $kg^{-1}H_2O$ $decade^{-1}$, respectively, but the trends in other districts are

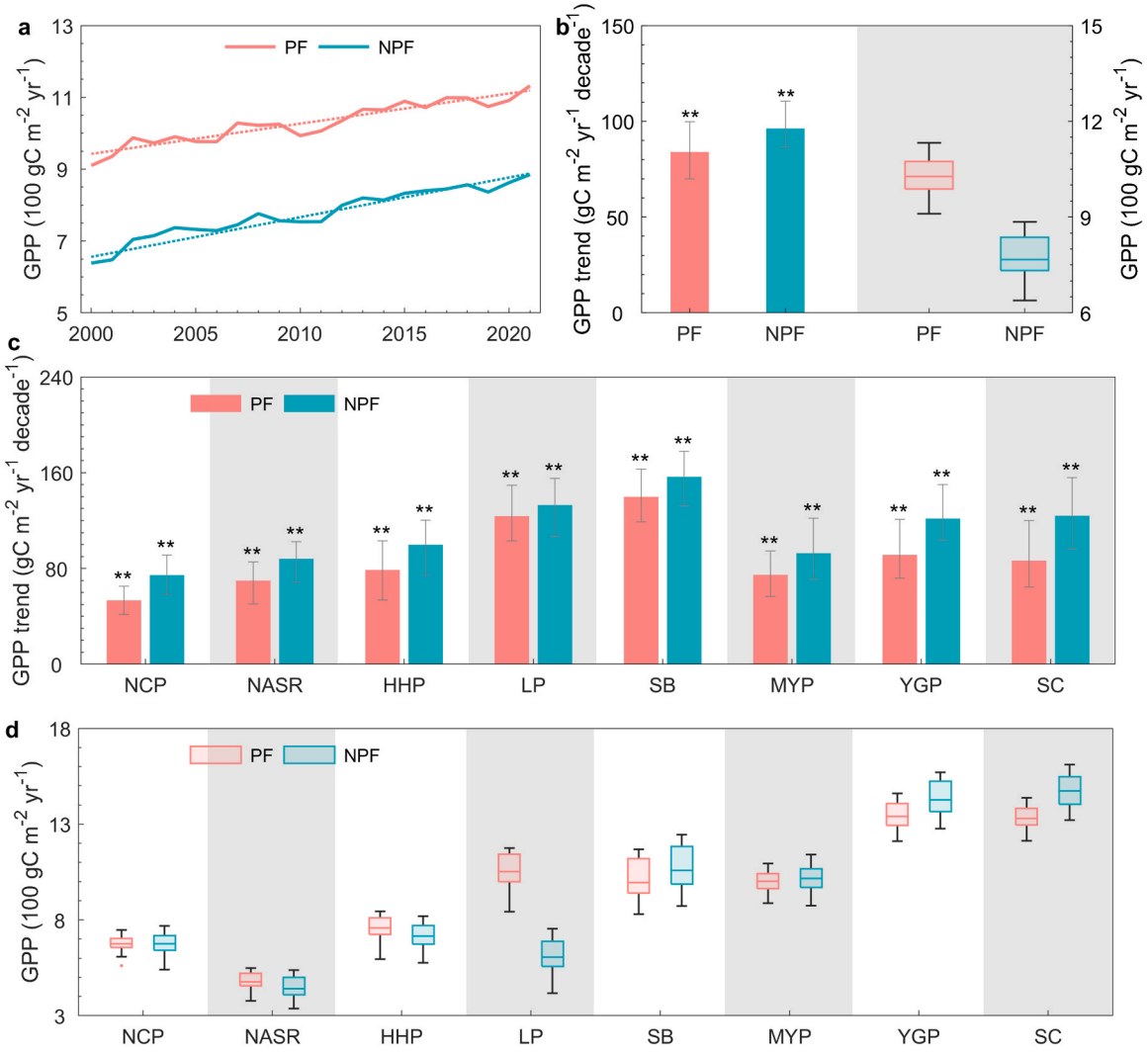

Fig. 6. Amount and trends in annual gross primary productivity (GPP) in paddy field (PF) and non-paddy field (NPF) over China during 2000–2021. (a) Time-series of annual GPP over whole China. (b) Trends and amount of GPP over whole China. c-d, Trends (c) and amount (d) of GPP in nine agricultural districts. The error bars in b and c represent standard error of the trends, and * * represents significant ET changes ($p < 0.01$) based on the Mann-Kendall trend test.

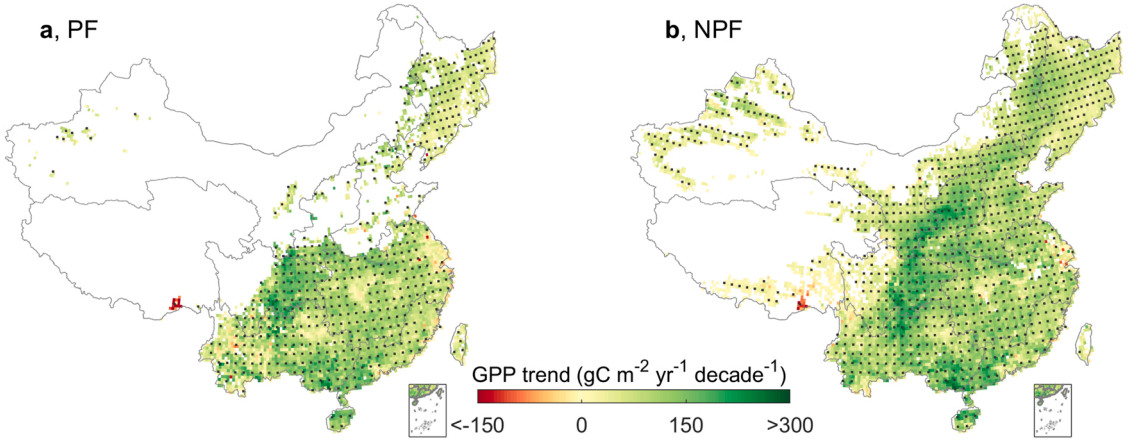

Fig. 7. Spatial variability of annual gross primarily productivity (GPP) trend in (a) paddy field (NPF) and (b) non-paddy field (NPF) cropland of China over the period of 2000–2021. The dotted grids represent significant GPP changes ($p < 0.05$) based on the Mann-Kendall trend test.

not significant (Fig. 9c). Spatial trends of seasonal WUE show substantial heterogeneity in both PF and NPF (Fig. S7), summer WUE presents overall decreasing trends in both PF and NPF of China. Spring WUE in the middle of the China cropland (LP, SB, north of the MYP) and autumn WUE in southern China presents a significant decreasing trend, but an overall increasing WUE trend is observed for winter.

Table 2
Contributions (in %) of seasonal paddy field (PF) and non-paddy field (NPF) gross primarily productivity (GPP) variation across the nine agricultural districts to total GPP change of China.

Types	Season	Nine agricultural districts of China									China
		NCP	NASR	HHP	LP	QTP	SB	MYP	YGP	SC	
PF	Spring	0.7	0.0	0.8	1.1	0.0	8.0	15.8	6.9	3.6	36.8
	Summer	4.8	0.8	1.3	1.1	0.0	4.5	6.8	-0.2	1.2	20.2
	Autumn	1.5	0.2	0.8	0.4	0.0	6.0	13.0	3.2	0.8	25.8
	Winter	0.0	0.0	0.2	0.2	0.0	2.0	6.7	4.1	4.0	17.2
NPF	Spring	1.9	2.3	8.0	2.6	0.1	4.7	3.8	5.0	0.9	29.2
	Summer	10.0	11.1	7.5	6.6	0.2	3.0	1.5	0.7	0.4	41.1
	Autumn	3.4	3.3	4.1	2.1	0.1	3.1	2.2	2.5	0.3	21.1
	Winter	0.0	0.1	2.1	0.3	0.0	1.3	1.5	2.3	1.0	8.6

Note: Northeast China Plain (NCP), Yunnan-Guizhou Plateau (YGP), Northern arid and semiarid region (NASR), Southern China (SC), Sichuan Basin and surrounding regions (SB), Middle-lower Yangtze Plain (MYP), Qinghai Tibet Plateau (QTP), Loess Plateau (LP) and Huang-Huai-Hai Plain (HHP).

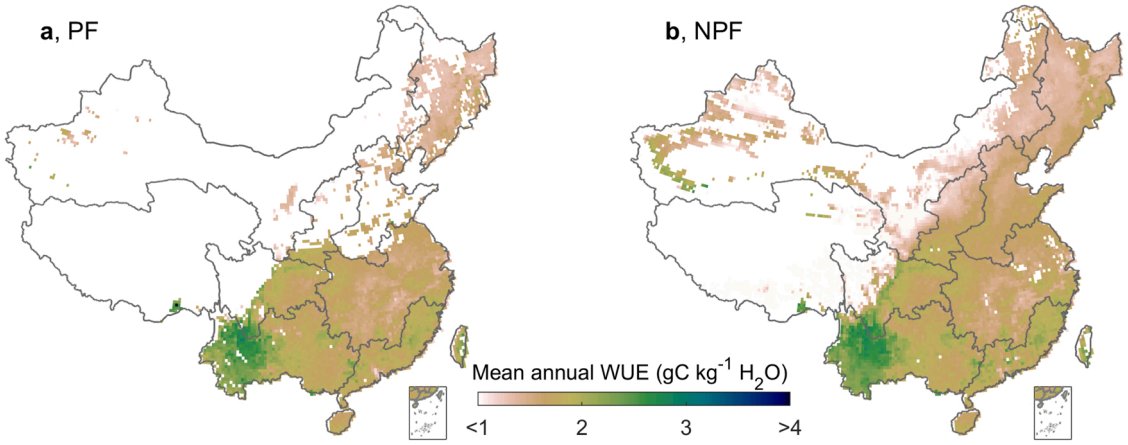

Fig. 8. Spatial variability of estimated mean annual water use efficiency (WUE) in (a) paddy field (NPF) and (b) non-paddy field (NPF) of China over the period of 2000–2021.

4. Discussion

4.1. Spatial patterns and trend of cropland ET

The spatial patterns of mean annual ET displayed the rising patterns from northwest to southeast across China, and the patterns were caused by the interaction of multiple influencing factors—basically demand (i.e., temperature, wind speed and water vapor deficit), supply (i.e. rainfall or soil water content) and energy (radiation and soil heat flux) (Cheng et al., 2021; Huang et al., 2015; Lan et al., 2021b). YGP, SC and MYP are located in a low-latitude coastal area, where the vegetation cover is high, together with the high water vapor transportation and sufficient energy, thus the ET rates were higher in these regions. While in north-eastern China (NASR and LP), despite the energy supply is sufficient for the ET process, it is difficult to transport water vapor because of its inland location. Inadequate water supply (low precipitation and soil moisture) restricts the underlying water loss. The conditions of the NCP are similar to those of the NASR, but cropland ET exhibited seasonal characteristics in these regions. High snow cover and low vegetation cover limited the cropland ET in winter, but the ET rate was relatively higher in summer due to the precipitation being more abundant (Fig. S2d).

Annual ET values in PF were higher than that of NPF in north China, but the value of the two was comparable in south China. Most regions in north China belong to arid or semi-arid areas, where soil moisture is the dominant constraint factor for the ET process (Bai et al., 2019; Yu et al., 2020). Soil water can be supplied by irrigation except for precipitation, therefore, ET in PF was higher than that of NPF, especially in LP (Fig. 3). However, crop irrigation demands were low in south China, and can even be achieved under optimal use of the plenty of natural rainfall (Luo et al., 2022), therefore, the difference between PF and NPF annual ET was small in south China. The estimated annual ET value is 625 $\pm$ 43 mm yr^{-1} in PF and 487 $\pm$ 45 mm yr^{-1} in NPF from 2000 to 2021. The values were larger than the reported ET value (359.61 mm yr^{-1}) based on MOD16 in 2000–2018 for the vegetated area of China (Cheng et al., 2021), demonstrating a stronger water loss process in the cropland ecosystem.

Detection of the ET trend in croplands can offer valuable information for land use and water resource management in changing climates. Our study has revealed that national cropland ET showed an overall rising trend during the time of 2000–2021. These findings are following some previous global and regional reports (Jiang et al., 2020b; Jung et al., 2010; Li et al., 2018; Liu et al., 2022; Xu et al., 2018; Yang et al., 2021; Zeng et al., 2018a). Recently, regional and global studies have also attributed the significantly increased ET to vegetation greening and increased precipitation (Lawrence and Vandecar, 2015; Ogutu et al., 2021). Bai et al. (2020) found that ET increased over nearly three quarters of China due to vegetation greening, Lan et al. (2021a) revealed that vegetation greening contributed most to increased ET in China from 2001 to 2015. The results agreed well with those reported for the Yellow River Basin (Jiang et al., 2020b; Yang et al., 2021), North China Plain (Liu et al., 2020b) and Loess Plateau (Bai et al., 2020), where ET increased with the vegetation greening. Yuan et al. (2021) explored the potential mechanism underlying the effect of vegetation dynamics on ET using a physical model, and the results revealed that vegetation greening reduced surface albedo, aerodynamic conductance and canopy stomatal conductance, resulting in an increase of ET. Greening has been proven to contribute a 32 % net increase in leaf area of China cropland due to intensive management over the last three decades (Chen et al., 2019; Forzieri et al., 2020). Increased vegetation cover affected ET by

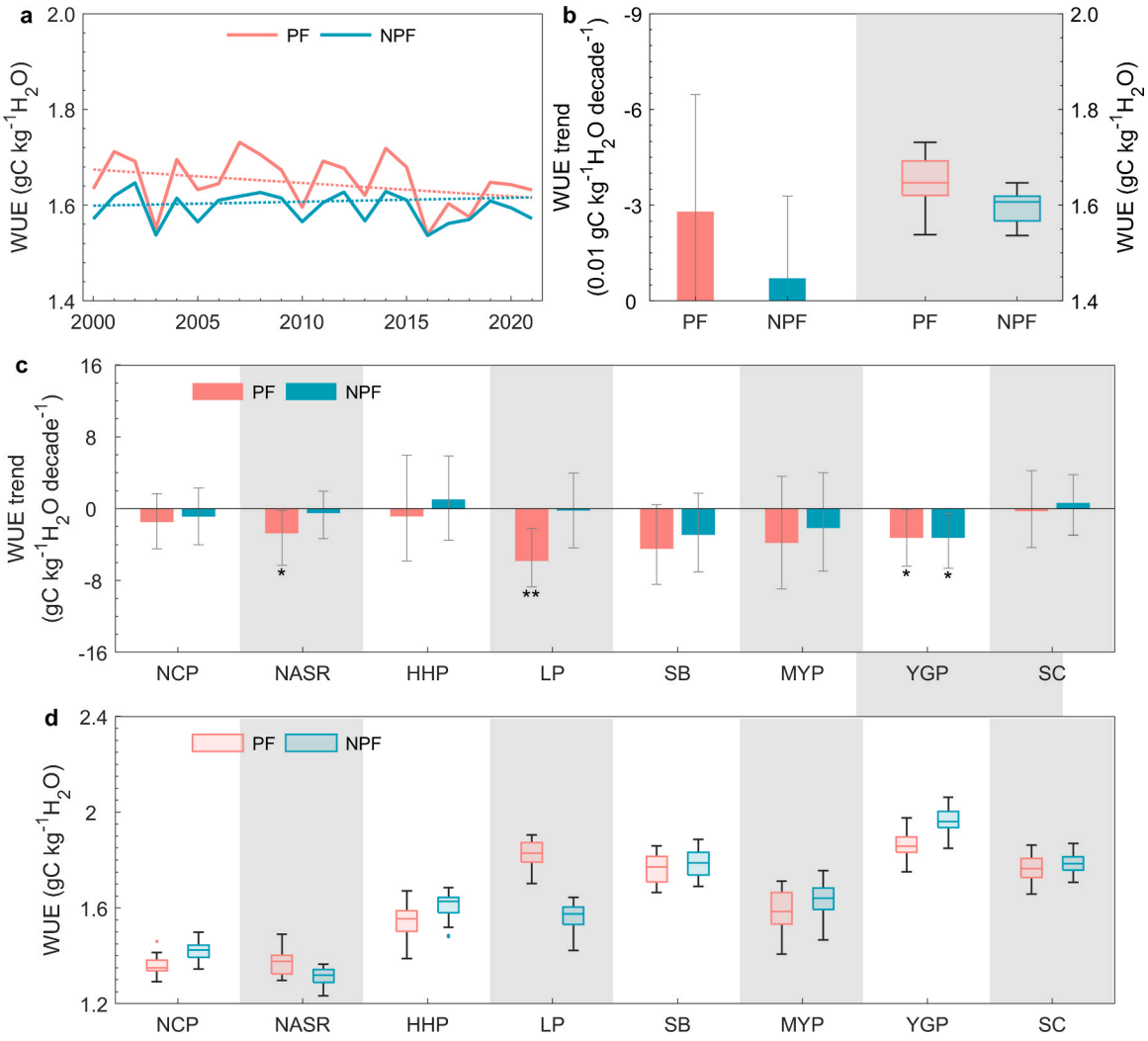

Fig. 9. Amount and trends in annual water use efficiency (WUE) in paddy field (PF) and non-paddy field (NPF) over China during 2000–2021. (a) Time-series of annual WUE over whole China. (b) Trends and amount of WUE over whole China. c-d, Trends (c) and amount (d) of WUE in nine agricultural districts. The error bars in b and c represent standard error of the trends, and * * represents significant ET changes ($p < 0.01$) based on the Mann-Kendall trend test.

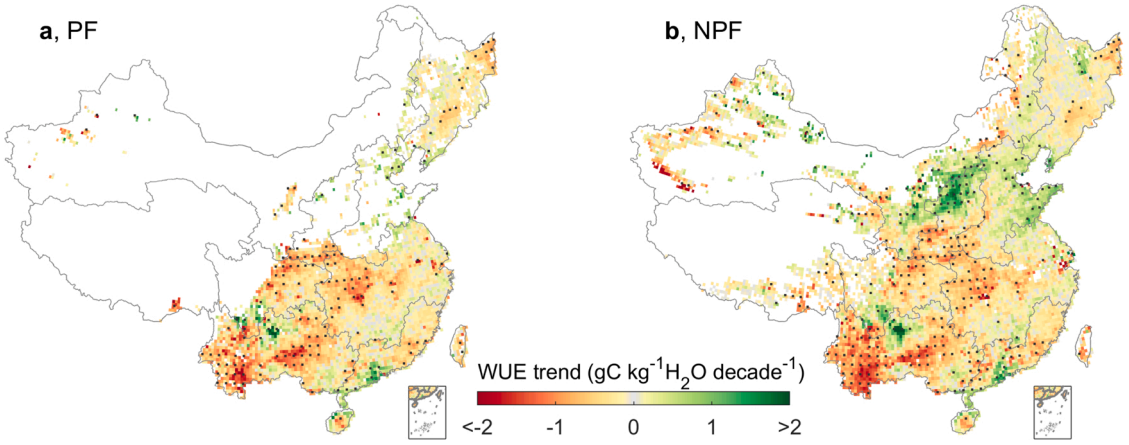

Fig. 10. Spatial patterns of trends in annual water use efficiency (WUE) trend in (a) paddy field (NPF) and (b) non-paddy field (NPF) of China over the period of 2000–2021. The dotted grids represent significant WUE changes ($p < 0.05$) based on the Mann-Kendall trend test.

increasing plant transpiration and intercepted rainfall evaporation (Zhang et al., 2015; Zheng et al., 2022). Besides, annual precipitation has been proven to increase in China in recent years (Yu et al., 2020), which supplies water source for potential atmospheric demand, especially for the NPF of arid and semi-arid regions (Su et al., 2021; Zheng et al., 2022). All the aforementioned factors supported the upward ET

trend in our study. However, the dominant driver factors and their contribution to rising ET are not uniform across the regions and the seasons. For example, ET in summer increases more than in other seasons, previous study also showed that an increase in reference ET in summer has a similar magnitude to that of spring, and is much larger than those in autumn and winter, due to increasing air temperature and decreasing relative humidity (Jin et al., 2022). Therefore, the factors driving ET variation remain to clarify in China cropland.

The magnitude of changes in NPF ET is higher than of PF. The estimated magnitude of increased annual ET is more drastic than national ET trend of 29.5 mm yr^{-1} $decade^{-1}$ in China from 2000 to 2018 (Cheng et al., 2021). The trend of ET in cropland was also greater than that of forest and grassland reported in China (Cheng et al., 2021), indicating the important positive role of cropland contribution to the national and global terrestrial water cycle. Terrestrial precipitation also showed a positive trend of 0.66 mm yr^{-2} in mainland China over the same period, which is consistent with the intensified water cycle in a warming climate due to greater atmospheric demand. However, the trend is much lower than the increase of ET, which contributed to the reduction in soil moisture (Zhang et al., 2015) and increased risk of agricultural drought (Liu et al., 2022; Wouters et al., 2022). In the content of the sustained rising ET, strategies can be formulated from the aspects of drought-resistant crop cultivation, planting structure adjustment, and water-saving irrigation technologies improvement, to hedge the negative effects of climate change on agriculture productivity (Liu et al., 2022; Madadgar et al., 2017; Yang et al., 2017), especially in the northern regions of China (Deng et al., 2021).

4.2. Spatial distribution and trend of GPP

The spatial distribution and variations of PF and NPF GPP were agreed well with annual ET, namely cropland with the higher ET also had larger GPP due to the coupled relationship between the two (Ogutu et al., 2021; Wagle et al., 2021). The estimates of mean annual GPP values in cropland fall within the reasonable reports for the Asian region (Ai et al., 2020). The value of NPF was comparable to the national mean value of 738.97 gC·m^{-2} yr^{-1} estimated from 2001 to 2015 in China (Lan et al., 2021b), the productivity in PF was higher than the national value, indicating the important positive role of PF in China terrestrial carbon sequestration.

The significant increasing trend of annual GPP is consistent with some studies published previously (Ai et al., 2020; Lan et al., 2021b). The increased rates of annual GPP were higher than the national annual GPP changes of 25.3 gC·m^{-2} yr^{-1} $decade^{-1}$ from 2001 to 2015 (Lan et al., 2021b), demonstrating that cropland plays an increasingly important role in China's terrestrial carbon sink. The rising temperature has been suggested to promote cropland vegetation growth and ecosystem productivity (Ciais et al., 2019; Keenan et al., 2013), especially for high-latitude regions (Dang et al., 2022; Yuan et al., 2020). Regional warming can length the crop growing season, allowing both earlier planting and later harvesting, prolongation of the seasonal nonfreezing period, and higher northern latitude regions expansion for planting (Liu et al., 2021; Yuan et al., 2020). Our study also found spring GPP increases contributed to the growth in annual GPP, with the value of 36.8 % and 29.2 % in PF in NPF, respectively. Autumn GPP increases contributed 25.8 % and 21.1 % of annual GPP increases in PF in NPF, respectively, probably because of the promoted crop growth and lengthened growing seasons.

Similar to vegetation greening, precipitation can strongly affect GPP by providing suitable moisture conditions, especially in water-limited regions (Guo et al., 2015). Modeling studies indicated that enhanced ET with vegetation greening can accelerate the atmospheric moisture recycle and therefore affect regional precipitation (Yao et al., 2018; Zeng et al., 2018b). Global climate model simulations also indicated that China's greening contributed to a significant increase of precipitation, especially for northern high latitudes (Zeng et al., 2018b). The increased GPP during the summer months (41.09 %) contributed a large increase to annual GPP in NPF, independent of growing season length, and the increasing trend was stronger in arid and semi-arid regions of northern China (10.0 % in NCP, 11.1 % in NASR, 7.5 % in HHP and 6.6 % in LP, Table 2). The increase in summer precipitation may explain for summer GPP increase in northern China, especially for NPF (Yu et al., 2020). Unignorably, elevated atmospheric CO_2 concentrations (CCO_2) stimulate carboxylation to enhance photosynthesis, and was also recognized as a favorable factor in enhancing vegetation productivity by its fertilization effects (Huang et al., 2015), although it showed a decline effect due to the limitations of water and nutrient composition in recent years (Wang et al., 2020; Zheng et al., 2022). The dominant driver factors affecting GPP variation are complex and not uniform across the regions, the detailed and quantitative assessments of factors affecting annual and seasonal GPP variations are still needed in the future.

4.3. WUE linking water and carbon

As a vital linkage of ecosystem carbon and water cycles, WUE can quantify the tradeoff between carbon sequestration and water consumption. The mean annual PF WUE was 1.65 gC $kg^{-1}H_2O$, which was comparable to the PF observed globally and higher than the national estimates of 1.42 gC $kg^{-1}H_2O$ from 2001 to 2015 (Ai et al., 2020; Lan et al., 2021b). In a similar study conducted in China and India, the results showed the mean WUE was 1.0–1.5 gC m^{-2} $kg^{-1}H_2O$, which is lower than our estimates (Ai et al., 2020). Besides, annual WUE in PF was slightly higher than in NPF, indicating PF is generally better than NPF as far as water conditions and management practice. Therefore, potential productivity in PF is superior to NPF (Jin et al., 2018). For example, the agricultural industry in the LP is strongly dependent on irrigation practices, so the WUE of PF farmland is significantly higher than that of NPF (Fig. 9). Besides, differences and variations of WUE in terrestrial ecosystems are related to differences in environmental responsiveness between the water and the carbon cycles, and human activities (i.e., irrigation, fertilizer application) (Jin et al., 2018; Ogutu et al., 2021).

The investigation of cropland WUE trend showed that, overall, cropland WUE decreased in China, though the trends were not uniform and disparities existed across the sub-agricultural districts (Fig. 10). Since WUE was estimated as GPP/ET, this negative WUE trend implied a large increase in ET not matched the enhancement in GPP in both PF and NPF of China. The decreased annual WUE was consistent with the results reported in some regions of China (Jin et al., 2018; Qin et al., 2013), as they found that a sustained increase of ET could result in increased water stress, which can limit GPP and finally decrease WUE in NPF, especially in a water-limited environment (Cheng et al., 2017; Ogutu et al., 2021). Yu et al. (2020) found ET and soil moisture trends are opposed in most regions of China, because ET remains primarily demand-limited due to increasing atmospheric demand. Therefore, the depleted soil moisture reduced the capacity for vegetation carbon assimilation, but not to the extent of restricting ET (Deng et al., 2021; Reichstein et al., 2002). The adverse effects of warm droughts also were found to limit GPP increases in eastern China during the period of 2000–2016 (Gampe et al., 2021). However, increased WUE may be found when sufficient soil moisture can be compensated for the enhanced cropland ET. For example, Yu et al. (2022) found that precipitation increased significantly in the northern LP, while an insignificant decrease was found in the southern LP, the compensated soil moisture in northern LP may be the reason causing the opposite trend of annual WUE between northern and southern NPF in LP (Fig. 10) (Yu et al., 2020).

As for the seasonal WUE trend, previous studies have found vegetation greening and beforehand growing season exacerbated the tendency of soil drying in northern and northwestern China (Liu et al., 2020a), which explained the decreased WUE in spring and summer (Fig. S6). Ogutu et al. (2021) also found vegetation greening resulted in a larger enhancement in ET than that of GPP, causing a reduced WUE in

the western Sahel Sudano-Guinean region. However, a warmer climate favors surface crop growth in winter, which may explain the enhanced WUE in most regions of China (Fig. S6g,h) (Deng et al., 2020; Huang et al., 2015).

However, some different WUE trends were detected, part of them is due to the differences in the data sources, time-series lengths and study areas (Ai et al., 2020; Traore et al., 2014). Global scale and regional studies on WUE have documented a continued increase in terrestrial land WUE since the mid-1990 s due to the increases in atmospheric CCO_2 and greening (Cheng et al., 2017). The increase in GPP originates from the direct acceleration of photosynthesis in response to the rising CCO_2. Meanwhile, leaf transpiration rate was reduced resulting from the reduced stomatal conductance under rising CCO_2 from 1982 to 2015 (Wang et al., 2020). However, transpiration loss at the ecosystem scale may not reduce due to the enhancement of LAI, which can cause larger surface conductance. Besides, the larger LAI may cause a larger shaded leaf area, characterized by consuming larger water but not contributing the same carbon. Many studies addressed that increased T/ET contributed to enhanced WUE under vegetation greening (WUE=GPP/ET can be divided into WUE=GPP/T × T/ET) (Hu et al., 2008; Zheng et al., 2022). However, the increased T/ET may not evident when LAI attained a certain level (Hu et al., 2008). Recent studies also point WUE was mainly regulated by atmospheric evaporative demand and leaf stomatal conductance with little effect on LAI. Therefore, the decreased transpiration use efficiency (i.e., GPP/T) may be another reason for decreasing WUE under higher VPD conditions (Hu et al., 2008; Rigden et al., 2020). Hu et al. (2008) also found both GPP and ET were negatively correlated with WUE in an alpine swamp meadow ecosystem, where low transpiration use efficiency (i.e. GPP/T), which was affected by the leaf stomatal conductance and VPD, caused the low WUE (Hu et al., 2008).

4.4. Applications and implications

This study investigated the spatial-temporal variations of annual and seasonal ET, GPP and WUE in PF and NPF of China during 2000–2021, some suggestions for future work need to be identified. The first is that the uncertainty of data quality is a noteworthy problem. The MODIS products are greatly affected by the algorithm performance, which depends on the accuracy of vegetation cover, meteorological data, etc., (Mu et al., 2007; Turner et al., 2006). Most of the researchers confirmed that the ET values based on MODIS performed well based on EC flux data and grid evaluation (Velpuri et al., 2013). However, for MODIS GPP, although some researchers reported the data was sufficiently accurate by comparison with the site measurement and other datasets (NASA Bigfoot) in cropland, the underestimation results were found compared with EC in cropland due to different photosynthetic capacity between C_3 and C_4 species. Therefore, more accurate species-distribution products are urgent to estimate regional and global GPP (Yuan et al., 2015). In addition, ε_{max} in the algorithm of MODIS GPP remains constant for each vegetation species, it is highly variable between the different species, especially between C_3 and C_4 species (Turner et al., 2006). Thus, further improvement in the GPP algorithm and its parameters is necessary for accurate GPP estimates.

We used a static cropland map for the year 2010 to quantify cropland extent. The static map cannot describe the cropland dynamic during 2001–2021, which may partially affect the conclusions drawn. We further assessed the cropland dynamic from 1985 to 2015 using the same land cover map from the Resource and Environment Science and Data Center. We found the cropland area shows little change from 1985 to 2015, ranging from 177 to 179 Mha (Fig. S8). So, the effects of dynamic cropland area on water and carbon cycles can be ignored. Our study compared water and carbon cycles in PF and NPF fields, but ignored the role of plastic mulch in regulating the cycles in croplands. Although the satellite-based products can describe the water and carbon processes under plastic mulch, they can't accurately differentiate the processes in covered and non-covered croplands, as current satellite-based products have difficulties in quantifying the plastic mulch. Field studies have already showed that plastic mulch substantially enhance soil water and thermal processes in croplands, thus altering water, energy, and carbon cycles (Gong et al., 2015; Feng et al., 2019), and resulting in higher water use efficiency (Gong et al., 2017). Plastic mulch is widely applied in northern China, e.g., the Loess Plateau, Northwest China, and Northeast China. Thus, Further studies should combine plastic mulch maps with satellite observations to further investigate how plastic mulch regulate water and carbon cycles in croplands at regional and national scales.

Although we analyzed the variation of ET, GPP and WUE combined with the previous study, the driving mechanism of ET, GPP and WUE in cropland remain unclear. It is necessary to deeply explore and clarify the mechanism of hydro-meteorological variables and vegetation factors on WUE, and the specific influencing path of how external environmental variables affect WUE through influencing GPP and ET. Besides, many kinds of research have proven that, human activity is having a much greater influence on water resources than climate change in some regions (Dey and Mishra, 2017; Yang et al., 2018). For example, the transformation of large-scale dry cropland to PF in the past 10 years contributed to the increasing ET in northeastern China (Cheng et al., 2021). In addition, the increasing area of economic crops with high water consumption in China increased by 10.21 %, which may lead to a large growth in the overall ET (Pei et al., 2018). Therefore, the effect of human activities on water consumption should be taken into consideration in further study.

5. Conclusions

The magnitude of the contribution of croplands to the national carbon and water cycle is still currently unknown. The spatial-temporal variations of ET, GPP and WUE in cropland of China based on the MODIS products and cropland distribution data from 2000–2021 are investigated. The results are concluded as below:

1. Annual ET in both PF and NPF presented a spatially increasing trend from northwest to southeast of China. Annual ET is averaged at 625 $\pm$ 43 mm yr^{-1} in PF, and 487 $\pm$ 45 mm yr^{-1} in NPF during the study period. Annual ET experienced a significant increasing trend in China and all of the agricultural districts, with the overall rate of $66.7^{+10.9}_{-12.2}$ mm yr^{-1} $decade^{-1}$ in NPF and $59.8^{+16.6}_{-14.9}$ mm yr^{-1} $decade^{-1}$ in PF, and the magnitudes of increase in annual ET mainly comes from the ET increase in summer.
2. The spatial variations of annual GPP were well agreed with that of annual ET. Annual GPP was averaged at 1029 $\pm$ 57 gC m^{-2} yr^{-1} and 776 $\pm$ 67 gC m^{-2} yr^{-1}, with the significantly increased rate of $84.0^{+15.9}_{-14.2}$ gC m^{-2} $decade^{-1}$ and $96.3^{+14.2}_{-9.7}$ gC m^{-2} yr^{-1} $decade^{-1}$ ($p < 0.01$) in PF and NPF, respectively. The magnitudes of increase in spring GPP are responsible for increased annual GPP in PF, while the increased GPP in spring and summer contributed the most to increased annual GPP in NPF.
3. The mean annual WUE is 1.65 $\pm$ 0.05 and 1.59 $\pm$ 0.03 gC $kg^{-1}H_2O$, with the overall negative trends of $-$ 0.0285 gC $kg^{-1}H_2O$ $decade^{-1}$ and $-$ 0.0072 gC $kg^{-1}H_2O$ $decade^{-1}$ in PF and NPF, respectively ($p > 0.05$). Spring WUE in the middle of the China cropland (LP, SB, and north of the MYP) and summer WUE presented a significant decreasing trend, but an overall increasing WUE trend is observed for winter.

Declaration of Competing Interest

The authors declare that they have no known competing financial interests or personal relationships that could have appeared to influence the work reported in this paper.

Data Availability

All data are available online.

Acknowledgments

We are grateful to the Distributed Archive Center of Oak Ridge National Laboratory, and the Earth Observing System Data for making MODIS data available. This work was also financially funded by the National Key Research and Development Program of China (2021YFD1600803-1), Fundamental Research Funds for the Central Universities (YJ202259), and the Sichuan Province Science and Technology Support Program (23ZDYF3117, 2022YFN0021).

Appendix A. Supporting information

Supplementary data associated with this article can be found in the online version at doi:10.1016/j.agwat.2023.108427.

References

Ai, Z., Wang, Q., Yang, Y., Manevski, K., Yi, S., Zhao, X., 2020. Variation of gross primary production, evapotranspiration and water use efficiency for global croplands. Agric. For. Meteorol. 287, 107935.
Bai, M., Mo, X.G., Liu, S.X., Hu, S., 2019. Contributions of climate change and vegetation greening to evapotranspiration trend in a typical hilly-gully basin on the Loess Plateau, China. Sci. Total Environ. 657, 325–339.
Bai, P., Liu, X.M., Zhang, Y.Q., Liu, C.M., 2020. Assessing the impacts of vegetation greenness change on evapotranspiration and water yield in China. Water Resour. Res. 56.
Chen, C., Park, T., Wang, X., Piao, S., Xu, B., Chaturvedi, R.K., Fuchs, R., Brovkin, V., Ciais, P., Fensholt, R., Tommervik, H., Bala, G., Zhu, Z., Nemani, R.R., Myneni, R.B., 2019a. China and India lead in greening of the world through land-use management. Nat. Sustain. 2, 122–129.
Cheng, L., Zhang, L., Wang, Y.P., Canadell, J.G., Chiew, F.H.S., Beringer, J., Li, L., Miralles, D.G., Piao, S., Zhang, Y., 2017. Recent increases in terrestrial carbon uptake at little cost to the water cycle. Nat. Commun. 8, 110.
Cheng, M., Jiao, X., Jin, X., Li, B., Liu, K., Shi, L., 2021. Satellite time series data reveal interannual and seasonal spatiotemporal evapotranspiration patterns in China in response to effect factors. Agric. Water Manag. 255, 107046.
Ciais, P., Tan, J., Wang, X., Roedenbeck, C., Chevallier, F., Piao, S.L., Moriarty, R., Broquet, G., Le Quere, C., Canadell, J.G., Peng, S., Poulter, B., Liu, Z., Tans, P., 2019. Five decades of northern land carbon uptake revealed by the interhemispheric CO_2 gradient. Nature 568, 221–225.
Dang, C., Shao, Z., Huang, X., Qian, J., Cheng, G., Ding, Q., Fan, Y., 2022. Assessment of the importance of increasing temperature and decreasing soil moisture on global ecosystem productivity using solar-induced chlorophyll fluorescence. Glob. Chang Biol. 28, 2066–2080.
Deng, Y., Wang, S., Bai, X., Luo, G., Wu, L., Chen, F., Wang, J., Li, C., Yang, Y., Hu, Z., Tian, S., Lu, Q., 2020. Vegetation greening intensified soil drying in some semi-arid and arid areas of the world. Agric. For. Meteorol. 292–293.
Deng, Y., Wang, X.H., Wang, K., Ciais, P., Tang, S.C., Jin, L., Li, L.L., Piao, S.L., 2021. Responses of vegetation greenness and carbon cycle to extreme droughts in China. Agric. For. Meteor. 298.
Dey, P., Mishra, A., 2017. Separating the impacts of climate change and human activities on streamflow: a review of methodologies and critical assumptions. J. Hydrol. 548, 278–290.
Feng, Y., Gong, D., Mei, X., Hao, W., Tang, D., Cui, N., 2017a. Energy balance and partitioning in partial plastic mulched and non-mulched maize fields on the Loess Plateau of China. Agric. Water Manag. 191, 193–206.
Feng, Y., Cui, N., Du, T., Gong, D., Hu, X., Zhao, L., 2017b. Response of sap flux and evapotranspiration to deficit irrigation of greenhouse pear-jujube trees in semi-arid northwest China. Agric. Water Manag. 194, 1–12.
Feng, Y., Hao, W., Gao, L., Li, H., Gong, D., Cui, N., 2019. Comparison of maize water consumption at different scales between mulched and non-mulched croplands. Agric. Water Manag. 216, 315–324.
Feng, Y., Ziegler, A.D., Elsen, P.R., Liu, Y., He, X., Spracklen, D.V., Holden, J., Jiang, X., Zheng, C., Zeng, Z., 2021. Upward expansion and acceleration of forest clearance in the mountains of Southeast Asia. Nat. Sustain 4, 892–899.
Feng, Y., Zeng, Z., Searchinger, T.D., Ziegler, A.D., Wu, J., Wang, D., He, X., Elsen, P.R., Ciais, P., Xu, R., Guo, Z., Peng, L., Tao, Y., Spracklen, D.V., Holden, J., Liu, X., Zheng, Y., Xu, P., Chen, J., Jiang, X., Song, X., Lakshmi, V., Wood, E.F., Zheng, C., 2022. Doubling of annual forest carbon loss over the tropics during the early twenty-first century. Nat. Sustain. 5 (5), 444–451.
Ferreira, L.B., Cunha, F.F.D., 2020. New approach to estimate daily reference evapotranspiration based on hourly temperature and relative humidity using machine learning and deep learning. Agric. Water Manag. 234, 106113.
Forzieri, G., Miralles, D.G., Ciais, P., Alkama, R., Ryu, Y., Duveiller, G., Zhang, K., Robertson, E., Kautz, M., Martens, B., Jiang, C., Arneth, A., Georgievski, G., Li, W., Ceccherini, G., Anthoni, P., Lawrence, P., Wiltshire, A., Pongratz, J., Piao, S., Sitch, S., Goll, D.S., Arora, V.K., Lienert, S., Lombardozzi, D., Kato, E., Nabel, J.E.M. S., Tian, H., Friedlingstein, P., Cescatti, A., 2020. Increased control of vegetation on global terrestrial energy fluxes. Nat. Clim. Change 10, 356–362.
Gampe, D., Zscheischler, J., Reichstein, M., O'Sullivan, M., Smith, W.K., Sitch, S., Buermann, W., 2021. Increasing impact of warm droughts on northern ecosystem productivity over recent decades. Nat. Clim. Change 11, 772–779.
Gong, D., Hao, W., Mei, X., Gao, X., Liu, Q., Caylor, K., 2015. Warmer and wetter soil stimulates assimilation more than respiration in rainfed agricultural ecosystem on the China Loess Plateau: the role of partial plastic film mulching tillage. PLoS One 10 (8), e0136578.
Gong, D., Mei, X., Hao, W., Wang, H., Caylor, K.K., 2017. Comparison of multi-level water use efficiency between plastic film partially mulched and non-mulched croplands at eastern Loess Plateau of China. Agric. Water Manag. 179, 215–226.
Guo, Q., Hu, Z., Li, S., Yu, G., Sun, X., Zhang, L., Mu, S., Zhu, X., Wang, Y., Li, Y., Zhao, W., 2015. Contrasting responses of gross primary productivity to precipitation events in a water-limited and a temperature-limited grassland ecosystem. Agric. For. Meteorol. 214–215, 169–177.
He, Z., Lei, L., Zeng, Z.C., Sheng, M., Welp, L.R., 2020. Evidence of Carbon Uptake Associated with Vegetation Greening Trends in Eastern China. Remote Sens-Basel 12, 718.
Hu, Z.M., Yu, G.R., Fu, Y.L., Sun, X.M., Li, Y.N., Shi, P.L., Wangw, Y.F., Zheng, Z.M., 2008. Effects of vegetation control on ecosystem water use efficiency within and among four grassland ecosystems in China. Glob. Change Biol. 14, 1609–1619.
Huang, M., Piao, S., Sun, Y., Ciais, P., Cheng, L., Mao, J., Poulter, B., Shi, X., Zeng, Z., Wang, Y., 2015. Change in terrestrial ecosystem water-use efficiency over the last three decades. Glob. Change Biol. 21, 2366–2378.
Hussain, M.Z., Hamilton, S.K., Bhardwaj, A.K., Basso, B., Thelen, K.D., Robertson, G.P., 2019. Evapotranspiration and water use efficiency of continuous maize and maize and soybean in rotation in the upper Midwest US. Agric. Water Manag. 221, 92–98.
Jiang, S., Liang, C., Cui, N., Zhao, L., Liu, C., Feng, Y., Hu, X., Gong, D., Zou, Q., 2020a. Water use efficiency and its drivers in four typical agroecosystems based on flux tower measurements. Agric. For. Meteorol. 295, 108200.
Jiang, Z.Y., Yang, Z.G., Zhang, S.Y., Liao, C.M., Hu, Z.M., Cao, R.C., Wu, H.W., 2020b. Revealing the spatio-temporal variability of evapotranspiration and its components based on an improved Shuttleworth-Wallace model in the Yellow River Basin. J. Environ. Manag. 262, 110310.
Jin, N., Ren, W., Tao, B., He, L., Ren, Q., Li, S., Yu, Q., 2018. Effects of water stress on water use efficiency of irrigated and rainfed wheat in the Loess Plateau, China. Sci. Total Environ. 642, 1–11.
Jin, Y., Wang, D., Feng, Y., Wu, J., Cui, W., He, X., Chen, A., Zeng, Z., 2022. Decreasing relative humidity dominates a reversal of decreasing pan evaporation in mainland China after 1989. J. Hydrol. 608, 127641.
Jin, Z., Liang, W., Yang, Y., Zhang, W., Yan, J., Chen, X., Li, S., Mo, X., 2017. Separating vegetation greening and climate change controls on evapotranspiration trend over the Loess Plateau. Sci. Rep. 7, 8191.
Ju, H., van der Velde, M., Lin, E., Xiong, W., Li, Y., 2013. The impacts of climate change on agricultural production systems in China. Clim. Change 120, 313–324.
Jung, M., Reichstein, M., Ciais, P., Seneviratne, S.I., Sheffield, J., Goulden, M.L., Bonan, G., Cescatti, A., Chen, J.Q., de Jeu, R., Dolman, A.J., Eugster, W., Gerten, D., Gianelle, D., Gobron, N., Heinke, J., Kimball, J., Law, B.E., Montagnani, L., Mu, Q.Z., Mueller, B., Oleson, K., Papale, D., Richardson, A.D., Roupsard, O., Running, S., Tomelleri, E., Viovy, N., Weber, U., Williams, C., Wood, E., Zaehle, S., Zhang, K., 2010. Recent decline in the global land evapotranspiration trend due to limited moisture supply. Nature 467, 951–954.
Keenan, T.F., Hollinger, D.Y., Bohrer, G., Dragoni, D., Munger, J.W., Schmid, H.P., Richardson, A.D., 2013. Increase in forest water-use efficiency as atmospheric carbon dioxide concentrations rise. Nature 499, 324–327.
Lan, X., Li, Y., Shao, R., Chen, X., Lin, K., Cheng, L., Gao, H., Liu, Z., 2021a. Vegetation controls on surface energy partitioning and water budget over China. J. Hydrol. 600, 125646.
Lan, X., Liu, Z., Chen, X., Lin, K., Cheng, L., 2021b. Trade-off between carbon sequestration and water loss for vegetation greening in China. Agric. Ecosyst. Environ. 319, 107522.
Lawrence, D., Vandecar, K., 2015. Effects of tropical deforestation on climate and agriculture. Nat. Clim. Change 5, 27–36.
Li, X., He, Y., Zeng, Z., Lian, X., Wang, X., Du, M., Jia, G., Li, Y., Ma, Y., Tang, Y., Wang, W., Wu, Z., Yan, J., Yao, Y., Ciais, P., Zhang, X., Zhang, Y., Zhang, Y., Zhou, G., Piao, S., 2018. Spatiotemporal pattern of terrestrial evapotranspiration in China during the past thirty years. Agric. For. Meteor. 259, 131–140.
Liang, L., Feng, Y., Wu, J., He, X., Liang, S., Jiang, X., Oliveira, G., Qiu, J., Zeng, Z., 2022. Evaluation of ECOSTRESS evapotranspiration estimates over heterogeneous landscapes in the continental US. J. Hydrol. 613, 128470.
Liu, X., Feng, X., Fu, B., 2020a. Changes in global terrestrial ecosystem water use efficiency are closely related to soil moisture. Sci. Total Environ. 698, 134165.
Liu, X., He, B., Guo, L., Huang, L., Yuan, W., Chen, X., Hao, X., Xie, X., Zhang, Y., Zhong, Z., Li, T., Chen, A., 2021. European carbon uptake has not benefited from vegetation greening. Geophys. Res. Lett. 48.
Liu, Y., Mo, X., Hu, S., Chen, X., Liu, S., 2020b. Attribution analyses of evapotranspiration and gross primary productivity changes in Ziya-Daqing basins, China during 2001-2015. Theor. Appl. Climatol. 139, 1175–1189.
Liu, Y., Lin, Y., Huo, Z., Zhang, C., Wang, C., Xue, J., Huang, G., 2022. Spatio-temporal variation of irrigation water requirements for wheat and maize in the Yellow River Basin, China, 1974-2017. Agric. Water Manag. 262.
Luo, W., Chen, M., Kang, Y., Li, W., Li, D., Cui, Y., Khan, S., Luo, Y., 2022. Analysis of crop water requirements and irrigation demands for rice: Implications for increasing effective rainfall. Agric. Water Manag. 260.

Madadgar, S., AghaKouchak, A., Farahmand, A., Davis, S.J., 2017. Probabilistic estimates of drought impacts on agricultural production. Geophys. Res. Lett. 44, 7799–7807.
Mann, H.B., 1945. Non-parametric tests against trend. Econometrica 13, 245–259.
Monteith, J.L., 1965. Evaporation and environment. S. E. B. Symp. 19, 205–234.
Mu, Q., Heinsch, F.A., Zhao, M., Running, S.W., 2007. Development of a global evapotranspiration algorithm based on MODIS and global meteorology data. Remote Sens. Environ. 111, 519–536.
Mu, Q., Zhao, M., Running, S.W., 2011. Improvements to a MODIS global terrestrial evapotranspiration algorithm. Remote Sens. Environ. 115, 1781–1800.
Ogutu, B.O., D'Adamo, F., Dash, J., 2021. Impact of vegetation greening on carbon and water cycle in the African Sahel-Sudano-Guinean region. Glob. Planet. Change 202.
Pei, Y., Li, X., Yang, M., 2018. Changes in irrigated areas and the types of cropland in China Since 2000. J. Irrig. Drain. Eng. 37 (04), 1–8.
Piao, S., Ciais, P., Huang, Y., Shen, Z., Peng, S., Li, J., Zhou, L., Liu, H., Ma, Y., Ding, Y., Friedlingstein, P., Liu, C., Tan, K., Yu, Y., Zhang, T., Fang, J., 2010. The impacts of climate change on water resources and agriculture in China. Nature 467, 43–51.
Piao, S., Wang, X., Park, T., Chen, C., Lian, X., He, Y., Bjerke, J.W., Chen, A., Ciais, P., Tommervik, H., Nemani, R.R., Myneni, R.B., 2020. Characteristics, drivers and feedbacks of global greening. Nat. Rev. Earth Environ. 1, 14–27.
Qin, W., Chi, B., Oenema, O., 2013. Long-term monitoring of rainfed wheat yield and soil water at the Loess Plateau reveals low water use efficiency. Plos One 8.
Reichstein, M., Tenhunen, J.D., Roupsard, O., Ourcival, J.M., Rambal, S., Miglietta, F., Peressotti, A., Pecchiari, M., Tirone, G., Valentini, R., 2002. Severe drought effects on ecosystem CO_2 and H2O fluxes at three Mediterranean evergreen sites: revision of current hypotheses? Glob. Change Biol. 8, 999–1017.
Rigden, A.J., Mueller, N.D., Holbrook, N.M., Pillai, N., Huybers, P., 2020. Combined influence of soil moisture and atmospheric evaporative demand is important for accurately predicting US maize yields. Nat. Food 1, 127–133.
Running, S.W., Nemani, R.R., Heinsch, F.A., Zhao, M.S., Reeves, M., Hashimoto, H., 2004. A continuous satellite-derived measure of global terrestrial primary production. Bioscience 54, 547–560.
Sen, P.K., 1968. Estimates of the regression coefficient based on Kendall's tau. J. Am. Stat. Assoc. 63, 1379–1389.
Su, T., Feng, T., Huang, B., Han, Z., Qian, Z., Feng, G., Hou, W., 2021. Trend, seasonal, and irregular variations in regional actual evapotranspiration over China: a multi-dataset analysis. Front. Phys. 9.
Traore, A.K., Ciais, P., Vuichard, N., MacBean, N., Dardel, C., Poulter, B., Piao, S., Fisher, J.B., Viovy, N., Jung, M., Myneni, R., 2014. 1982-2010 trends of light use efficiency and inherent water use efficiency in African vegetation: sensitivity to climate and atmospheric CO_2 concentrations. Remote Sens-Basel 6, 8923–8944.
Turner, D.P., Ritts, W.D., Maosheng, Z., Kurc, S.A., Dunn, A.L., Wofsy, S.C., Small, E.E., Running, S.W., 2006. Assessing interannual variation in MODIS-based estimates of gross primary production. IEEE T. Geosci. Remote 44, 1899–1907.
Velpuri, N.M., Senay, G.B., Singh, R.K., Bohms, S., Verdin, J.P., 2013. A comprehensive evaluation of two MODIS evapotranspiration products over the conterminous United States: Using point and gridded FLUXNET and water balance ET. Remote Sens. Environ. 139, 35–49.
Wagle, P., Gowda, P.H., Northup, B.K., Neel, J.P.S., 2021. Ecosystem-level water use efficiency and evapotranspiration partitioning in conventional till and no-till rainfed canola. Agric. Water Manag 250, 106825.
Wang, S., Zhang, Y., Ju, W., Chen, J.M., Ciais, P., Cescatti, A., Sardans, J., Janssens, I.A., Wu, M., Berry, J.A., Campbell, E., Fernandez-Martinez, M., Alkama, R., Sftch, S., Friedlingstein, P., Smith, W.K., Yuan, W., He, W., Lombardozzi, D., Kautz, M., Zhu, D., Lienert, S., Kato, E., Poulter, B., Sanders, T.G.M., Kruger, I., Wang, R., Zeng, N., Tian, H., Vuichard, N., Jain, A.K., Wiltshire, A., Haverd, V., Goll, D.S., Penuelas, J., 2020. Recent global decline of CO_2 fertilization effects on vegetation photosynthesis. Science 370, 1295–1300.
Wouters, H., Keune, J., Petrova, I.Y., van Heerwaarden, C.C., Teuling, A.J., Pal, J.S., Vila-Guerau de Arellano, J., Miralles, D.G., 2022. Soil drought can mitigate deadly heat stress thanks to a reduction of air humidity. Sci. Adv. 8, eabe6653.
Wu, J., Wang, D., Li, L.Z., Zeng, Z., 2022a. Hydrological feedback from projected Earth greening in the 21st century. Sustain. Horiz. 1, 100007.
Wu, J., Feng, Y., Liang, L., He, X., Zeng, Z., 2022b. Assessing evapotranspiration observed from ECOSTRESS using flux measurements in agroecosystems. Agric. Water Manag. 269, 107706.
Xu, S., Yu, Z., Yang, C., Ji, X., Zhang, K., 2018. Trends in evapotranspiration and their responses to climate change and vegetation greening over the upper reaches of the Yellow River Basin. Agric. For. Meteorol. 263, 118–129.
Yang, G., Xue, L., He, X., Wang, C., Long, A., 2017. Change in land use and evapotranspiration in the Manas River Basin, China with long-term water-saving measures. Sci. Rep. 7.
Yang, L., Feng, Q., Adamowski, J.F., Alizadeh, M.R., Yin, Z., Wen, X., Zhu, M., 2021. The role of climate change and vegetation greening on the variation of terrestrial evapotranspiration in northwest China's Qilian Mountains. Sci. Total Environ. 759, 143532.
Yang, P., Xia, J., Zhan, C., Chen, X., Qiao, Y., Chen, J., 2018. Separating the impacts of climate change and human activities on actual evapotranspiration in Aksu River Basin ecosystems, Northwest China. Hydrol. Res. 49, 1740–1752.
Yao, Y., Wang, X., Li, Y., Wang, T., Shen, M., Du, M., He, H., Li, Y., Luo, W., Ma, M., Ma, Y., Tang, Y., Wang, H., Zhang, X., Zhang, Y., Zhao, L., Zhou, G., Piao, S., 2018. Spatiotemporal pattern of gross primary productivity and its covariation with climate in China over the last thirty years. Glob. Change Biol. 24, 184–196.
Yu, L., Liu, Y., Liu, T., Yan, F., 2020. Impact of recent vegetation greening on temperature and precipitation over China. Agric. For. Meteorol. 295, 108197.
Yuan, F., Liu, J., Zuo, Y., Guo, Z., Wang, N., Song, C., Wang, Z., Sun, L., Guo, Y., Song, Y., Mao, D., Xu, F., Xu, X., 2020. Rising vegetation activity dominates growing water use efficiency in the Asian permafrost region from 1900 to 2100. Sci. Total Environ. 736, 139587.
Yuan, W., Cai, W., Nguy-Robertson, A.L., Fang, H., Suyker, A.E., Chen, Y., Dong, W., Liu, S., Zhang, H., 2015. Uncertainty in simulating gross primary production of cropland ecosystem from satellite-based models. Agric. For. Meteorol. 207, 48–57.
Yuan, X., Hamdi, R., Ochege, F., Kurban, A., De Maeyer, P., 2021. The sensitivity of global surface air temperature to vegetation greenness. Int. J. Climatol. 41, 483–496.
Zeng, Z., Peng, L., Piao, S., 2018a. Response of terrestrial evapotranspiration to Earth's greening. Curr. Opin. Env. Sust. 33, 9–25.
Zeng, Z., Piao, S., Li, L., Wang, T., Ciais, P., Lian, X., Yang, Y., Mao, J., Shi, X., Myneni, R., 2018b. Impact of Earth greening on the terrestrial water cycle. J. Clim. 31, 2633–2650.
Zhang, K., Kimball, J.S., Nemani, R.R., Running, S.W., Hong, Y., Gourley, J.J., Yu, Z., 2015. Vegetation greening and climate change promote multidecadal rises of global land evapotranspiration. Sci. Rep. 5, 15956.
Zheng, H., Miao, C., Li, X., Kong, D., Gou, J., Wu, J., Zhang, S., 2022. Effects of vegetation changes and multiple environmental factors on evapotranspiration across China over the past 34 years. Earths Future 10.